ACS APPLIED NANO MATERIALS

www.acsanm.org Article

Optical Properties and Nanocavity Response of $CsPbCl_3$ Nanowires: Implications for Light-Emitting Devices

Mohammad Kamal Hossain,* Szymon J. Zelewski, Robert Kudrawiec, Marcin Syperek, Roberto dos. Reis, Yuen Hong Tsang, Johnny C. Ho, and Kin Man Yu*

Cite This: *ACS Appl. Nano Mater.* 2025, 8, 23933−23944 Read Online

ACCESS | Metrics & More | Article Recommendations | Supporting Information

ABSTRACT: Advanced photochemical stability, excellent lasing response, and multifold higher nonlinear optical magnitude of all-inorganic $CsPbX_3$ (X = Cl, Br, and I) perovskites made them superior to their organic−inorganic hybrid halide counterparts and other conventional semiconducting materials. Herein, in addition to basic material properties, various aspects of the photoluminescence (PL) behaviors along with the highest ever *Q*-factor nanocavity response of $CsPbX_3$ (X = Cl) perovskite nanowires (NWs) are reported. The high-quality, single-crystalline $CsPbCl_3$ NWs were grown by the noncatalytic chemical vapor deposition (NC−CVD) approach. Strong violet-blue (∼415 nm) PL emission, excellent response to multiphoton absorption (MPA), and harmonic generation suggest that these NWs are suitable for light manipulation and detection-related miniaturized device applications. Temperature- and power-dependent PL measurements reveal that the PL emissions from the $CsPbCl_3$ NWs originate from excitonic transitions. Further, excitation fluence-dependent PL measurements on typical $CsPbCl_3$ NW demonstrate excellent single-mode lasing at $P_{Th} \sim 130\ \mu J/cm^2$ with a nanocavity response quality factor, $Q \sim 4500$, higher than most reported values for similar materials and nanostructures. We believe that, in addition to device miniaturization, these findings will surely advance and promote the one- and multiphoton absorption (OPA and MPA)-related optoelectronic applications of $CsPbX_3$ perovskites. Moreover, the insights of the photophysical transitions revealed here for large bandgap ($E_g \sim 2.99$ eV) $CsPbCl_3$ NWs may also facilitate the understanding of the photophysics of other wide bandgap semiconductors.

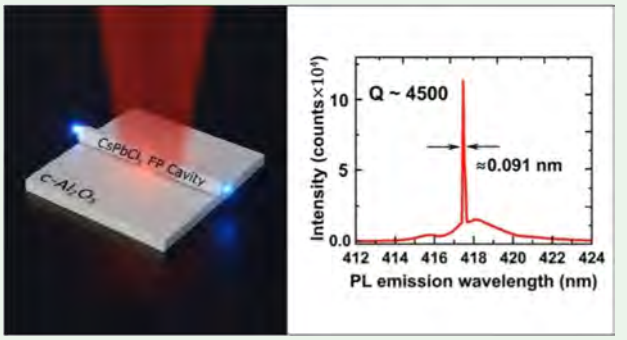

KEYWORDS: *all-inorganic halide perovskite nanowires, multiphoton absorption and harmonic generation, excitonic transition, single-mode lasing, high-Q cavity*

1. INTRODUCTION

Organic−Inorganic Hybrid Metal Halide Perovskites (OIMHPs) with their record power conversion efficiencies of 27.0%, 30.1%, and 34.9%, reported, respectively, for the single junction, perovskite tandem, and perovskite/Si hybrid tandem solar cells have attracted tremendous research interests as photovoltaic materials of the future.[1,2] However, easy ambient air and thermal degradation with limited bandgap tunability have impeded the large-scale deployment of these OIMHP-based high efficiency solar cells.[3] On the contrary, all-inorganic cesium lead halide perovskites, $CsPbX_3$ (X = Cl, Br, and I) demonstrate excellent stability against open-air oxygen, moisture, light, heat, and electric field.[4,5] In addition to the distinctive charge transport properties and a wide bandgap tunability, these all inorganic halide perovskites (AIHPs) also exhibit many intriguing optoelectronic properties including high photoluminescence (PL) quantum yield (∼90%), high charge carrier mobility (∼4500 $cm^2\ V^{-1}\ s^{-1}$), long charge carrier diffusion length (0.08−10 μm), and long carrier lifetime (1−25 ns).[6−9] These unique optoelectronic features of the pristine AIHPs are also reported to be tailored further by doping with various lanthanide and transition metal ions.[10−13] Moreover, for device applications, $CsPbX_3$ materials offer good potentials for highly stable and widely tunable nano/micro-lasers that serve the need of monochromatic power sources in many nano/microcompatible integrated optoelectronic and photonic applications.[14] With the above-mentioned desirable properties, AIHPs are considered highly prospective materials for future optoelectronic device applications.

At present, the miniaturization of photonic and optoelectronic devices is the priority concern for their potential incorporation into integrated circuits applications. The key factor that dictates device scale miniaturization is the

Received: September 9, 2025
Revised: November 28, 2025
Accepted: December 1, 2025
Published: December 9, 2025

https://doi.org/10.1021/acsanm.5c04170
ACS Appl. Nano Mater. 2025, 8, 23933−23944

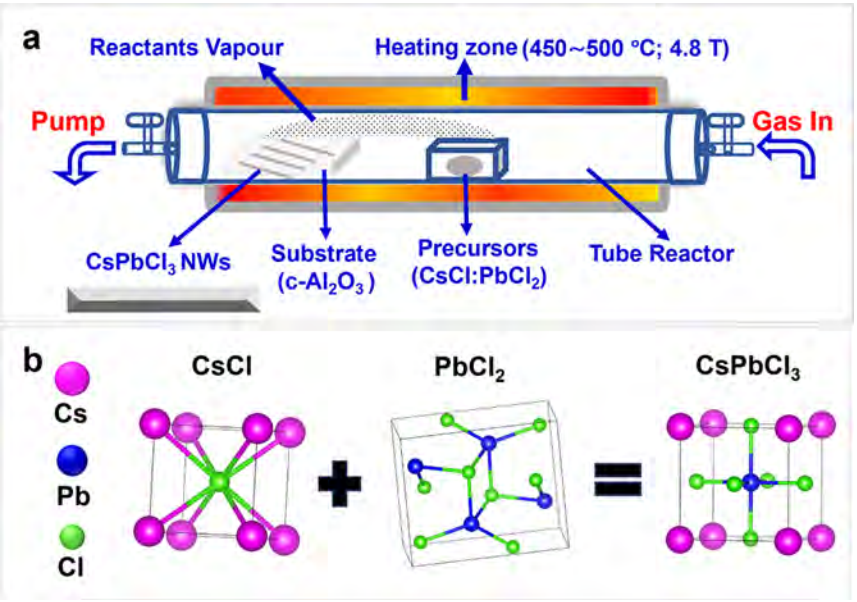

Figure 1. Materials Fabrication viewpoints of the noncatalytic chemical vapor deposition (NC−CVD) growth of all-inorganic $CsPbX_3$ (X = Cl) perovskite nanowires. (a) Schematic diagram illustrating the NC−CVD synthesis protocols for the growth of $CsPbCl_3$ NWs and (b) the chemical reaction involved in the NC−CVD growth of the $CsPbCl_3$ perovskite NWs.

dimensionality of the nanostructures. Also, dimensionality is considered to be the key factor for controlling the electron−matter and light−matter interactions, which in turn determine functionalities and the ultimate efficiency of the devices.[15] The one-dimensional (1D) semiconductor nanowire (NW) structures with their well-established anisotropic geometry, higher crystallinity, and charge confinement behavior show distinguishable optical properties over other nanoscale geometries.[16,17] Moreover, with rational design and controlled growth architectures, NW structures can offer certain unique electronic and photonic properties which are crucial for many sensitive optoelectronic devices.[18] For example, it has been reported that NWs with a triangular cross section exhibited a uniformly high-Q factor cavity response in a wider spectral range than that originated from other NW architectures.[4,8,19] Since AIHPs have already demonstrated high photoluminescence quantum yield (PLQY),[14] high external quantum efficiency,[16] low lasing threshold,[14,20] high quality factor (high-Q) cavity response,[14,20] and multifold higher multiphoton absorption (MPA) like nonlinear optical (NLO) response[21] over other traditional inorganic semiconductors, their high-quality triangular cross section single-crystalline NWs would, therefore, be ideal for widely tunable high-efficiency miniaturized laser applications as well as for fundamental photophysics research.

Two-/multiphoton absorption (TPA/MPA) is a NLO process that offers high spatial confinement of the incident radiation and thereby can penetrate deeper into the sample.[22,23] In addition, MPA allows the realization of the high harmonic generation without the strict obligation of the phase matching requirement.[24] Second harmonic generation (SHG), the lowest order nonlinear process, allows the direct study of the electronic and magnetic structures as well as the dynamical behavior of a material, which are crucial for designing various sensitive devices.[25] NLO materials are, therefore, widely used in various photosensitive applications including fluorescence microscopy, photodynamic therapy, optical data storage, optical power limiting, lithography, in vivo imaging, and ultrafast optical signals characterization.[21,26−28] For AIHP materials, up to date, TPA/MPA properties are only explored on nano/microcrystals, nanoplates, and nanorods of $CsPbBr_3$ and CsPb(Br/Cl) as well as quantum dots of $CsPbCl_3$.[26,29−32] However, in larger crystals, MPA and frequency upconversion efficiency are much reduced due to the absence of quantum confinement and surface enhancement effects. Also, for AIHP nanostructures, the phase control in the subwavelength dimension and challenges for achieving high nonlinear conversion efficiency make the MPA process difficult.[30,33] Therefore, to exploit the full potentials of $CsPbX_3$ as NLO materials for real-life applications, it is necessary to find the right geometrical architecture(s) with a stable crystalline phase. Consequently, among various morphological features, understanding of the NLO properties of the AIHPs triangular NWs grown by the NC−CVD method could be a topic of fundamental research interest today.

The widely reported high-quality amplified spontaneous emissions (ASE) and excellent lasing response of the all-inorganic $CsPbX_3$ perovskites made them potential candidates for future lasing applications.[14,34−37] Among various nano/microstructured $CsPbX_3$ perovskite lasers, their nanowire counterparts have high prospects for possible incorporation into the on-chip integrated optoelectronic and photonic circuits.[14] Moreover, the triangular prismatic-shaped NWs are found to facilitate excellent optical fields confinement effect and therefore are well-suited as high-quality nanocavity resonators.[7,31] Among many other prospects, nano/microcavities having both high-quality factor (high-Q) and small modal volume are considered to be the heart of efficient on-chip coherent laser sources and are found suitable for various sophisticated applications such as on-chip optical communications, high density data storage, and high-resolution biological imaging.[35,36,38] Single-mode laser at the nanoscale dimension also ensures stabilization of the nanodevices.[22,39] However, the comparatively lower quality factor (low-Q) and larger modal volume of the halide perovskites resonator cavities realized up

https://doi.org/10.1021/acsanm.5c04170
ACS Appl. Nano Mater. 2025, 8, 23933−23944

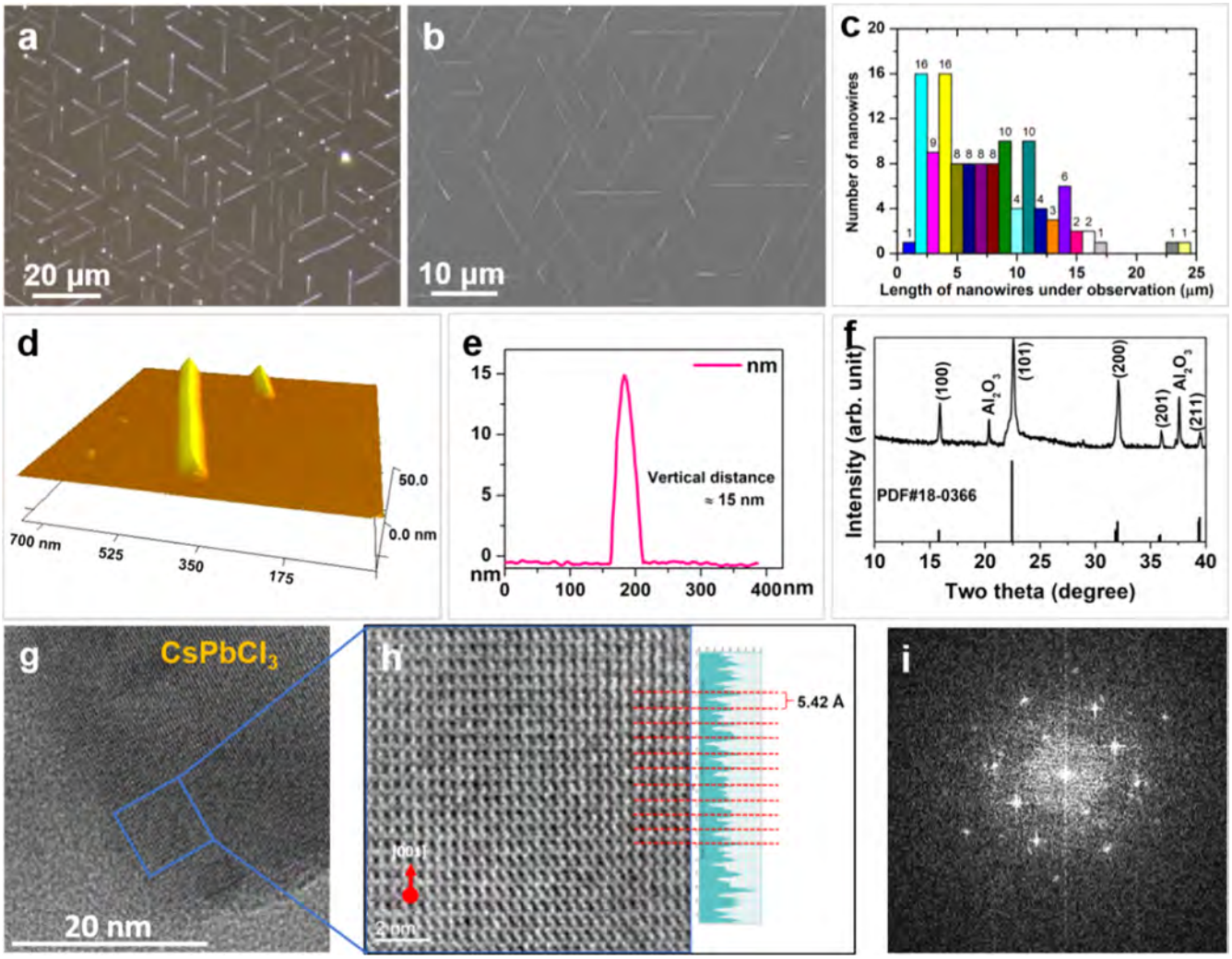

Figure 2. Morphology and crystalline property of all-inorganic $CsPbCl_3$ NWs. (a) Optical microscopy and (b) FESEM images of $CsPbCl_3$ NWs grown on the c-Al_2O_3 substrate. (c) Length distribution of the as-grown $CsPbCl_3$ NWs. (d,e) 3D AFM image showing triangular morphology and the corresponding height profile of $CsPbCl_3$ NWs. (f) X-ray diffraction patterns of $CsPbCl_3$ NWs. (g) High-resolution transmission electron microscopy (HRTEM) image of a $CsPbCl_3$ NW. (h) High-magnification view of the blue square part of Figure 2g and (i) corresponding FFT pattern obtained from the HRTEM image of the $CsPbCl_3$ NW.

to date restrict their applications in the frontiers of the nonlinear optics field.[31]

Here, we focus on the emission properties of $CsPbCl_3$ nanowires grown by the noncatalytic chemical vapor deposition (NC−CVD) technique[40] with particular emphasis on the lasing with a high quality factor and SHG. Our results suggest that these NWs are of high-quality single-crystalline nature and are good optical absorbers and emitters. The narrow, intense violet-blue (~415 nm) PL emission and excellent TPA/MPA responses along with SHG show $CsPbCl_3$ NW's potential for various light generation and manipulation applications. Moreover, both temperature- and power-dependent PL measurements suggest that the PL emissions from $CsPbCl_3$ NWs originate from the excitonic transitions. Excitation fluence-dependent PL measurements further demonstrate nonlinear dependency of the PL intensities on the excitation fluence. Excellent lasing with an extremely sharp single-mode lasing spectrum is realized for typical $CsPbCl_3$ NWs at a lasing threshold of ~130 $\mu J/cm^2$. Irrespective of the morphology and dimension, as well as the PL measurement temperature, the NWs show narrow line width ($\delta\lambda \sim 0.091$ nm), which results in a Q-factor value $Q \sim 4500$ for the nanocavity resonator, the highest reported, for this material. We believe that these findings promote the one- and multiphoton absorption-related cavity and gain medium applications of $CsPbX_3$ (X = Cl, Br, and I) perovskites as well as their device miniaturizations. The insights of the photophysical transition described here for $CsPbCl_3$ NWs ($E_g \sim 2.99$ eV) may also advance the understanding of the photophysics of other wide bandgap semiconductors and their nanostructures.

2. EXPERIMENTAL SECTION

2.1. Materials Preparation. $CsPbCl_3$ nanowires were grown by the noncatalytic chemical vapor deposition (NC−CVD) method (Figure 1). Commercially available high-purity cesium chloride (CsCl, 99.9%, Reagent Plus, Sigma-Aldrich) and lead(II) chloride ($PbCl_2$, 99%, Reagent grade, Alfa Aesar) were used as precursor materials as received without any further refinement. The growth was performed by using a home-built CVD setup that contains a tube reactor and a turbo pump system. CsCl and $PbCl_2$ reactants were mixed with 1:1 molar ratio and introduced to the furnace heating zone with a boron nitride boat. NWs were collected from the ultrasonically cleaned c-

https://doi.org/10.1021/acsanm.5c04170
ACS Appl. Nano Mater. 2025, 8, 23933−23944

Al_2O_3 substrates placed on the downstream side of the tube reactor of the CVD furnace. The growth was conducted in a sealed vacuum reactor environment with a base reactor pressure of ≤5 mT. High-purity Ar (99.99%) was introduced to the reactor at a rate of 100 sccm to purge the residuals, and finally, the growth pressure was adjusted and maintained to 4.8 T throughout the growth. The best growth was attained for the temperature range between 450 and 500 °C for a growth time of 40 min. The reactor was allowed to cool down naturally as soon as the growth was over.

2.2. Optical Measurements. For the macro-PL measurements, a He−Cd 325 nm CW laser with a typical spot size of ∼0.5 mm was used, and luminescence spectra were collected using a compact thermoelectrically cooled Si CCD spectrometer (Avantes). Low-temperature PL measurements were performed with samples placed in a closed-cycle He cryocooler. Temperature-dependent PL spectra were obtained with 10 K steps. For ultraviolet excitation, a beam from a tunable titanium-sapphire laser operating at the repetition frequency of 76 MHz (Coherent Mira 900) was frequency doubled to 380 nm. Both excitation beam and emitted photons were passed through a plan-apochromat 50x, NA = 0.55 microscope objective (spot size ∼5 μm). The PL signal was resolved with a 300 mm grating monochromator coupled with a liquid-nitrogen-cooled Si CCD array detector.

3. RESULTS AND DISCUSSION

In this work, we report on the distinctive properties and intriguing application prospects of the all-inorganic $CsPbCl_3$ perovskite NWs grown by the noncatalytic chemical vapor deposition (NC−CVD) approach shown in Figure 1. It is well established that NWs obtained from the NC−CVD growth have material properties superior to those obtained from the other traditional CVD growth approaches.[4,7,8,41] In brief, the catalytic CVD growth introduces foreign metal (catalyst) content into the growth products, which may be detrimental to the ultimate device performance.[7,8] In contrast, materials grown by the NC−CVD approach are free from these impurities and hence have higher purity, which in turn can enhance the performance of their final devices.[4,7,8,41] In the NC−CVD process, the growth was found to be initiated with vaporization of the metal halide precursors (CsCl/ $PbCl_2$), which then nucleated as $CsPbCl_3$ nanoparticles on the substrates placed at the downstream zone of the tube reactor. The $CsPbCl_3$ particles then went through several self-reorganization processes and formed longer chains. Finally, the chains connected together and the nanowires were formed.[40] The nanowires thus formed through the self-assembly mechanism instead of any NC−CVD grapho-epitaxial growth (Figure S1) reported earlier for the halide perovskite NWs.[5,41] Details of the NC−CVD growth of $CsPbX_3$ (X = Cl) NWs can be found in the article reported by Hossain et al.[40] Properties and application prospect of the $CsPbCl_3$ NWs are discussed chronologically in the following subsections.

3.1. Structural Properties of $CsPbCl_3$ NWs. The morphology and topography of $CsPbCl_3$ NWs grown on the c-Al_2O_3 substrate were investigated by optical microscopy and field emission scanning electron microscopy (FESEM). Typical optical and FESEM images of $CsPbCl_3$ NWs are shown in Figure 2a,b, respectively. Figure 2c shows the length distribution of the NWs, which mostly falls in the range of ∼2−14 μm. Interestingly, all of these NWs are found to be physically aligned with the hexagonal crystal facets of the c-Al_2O_3 substrate. High-resolution atomic force microscopy (AFM) image shown in Figure 2d reveals that the NWs have a triangular cross section with an average base and height dimension of ∼60 and ∼15 nm, respectively, as measured by the AFM line profile in Figure 2e. A very similar cross-sectional shape obtained for the AIHP $CsPbBr_3$ NWs grown on the c-Al_2O_3 substrate was also reported earlier in the literature.[40]

The X-ray diffraction (XRD) patterns of the $CsPbCl_3$ NWs are shown in Figure 2f. Low- and high-magnification, high-resolution transmission electron microscopy (HRTEM) images (Figure 2g,h) confirm the single-crystalline nature of the $CsPbCl_3$ NWs structures. The HRTEM image shown in Figure 2h further shows a lattice spacing of d = 0.54 nm, which closely matches with the (100) interplanar distance of the tetragonal crystal phase of the $CsPbCl_3$ perovskite.[4] The relevant XRD patterns and the fast Fourier transform (FFT) of the corresponding HRTEM image shown, respectively, in Figure 2f,i further confirm the tetragonal crystal structure of $CsPbCl_3$ NWs.

The crystalline homogeneity of the $CsPbCl_3$ NWs was studied by the confocal μ-Raman mapping using an excitation wavelength (energy) of λ_{exc} = 532 nm (∼2.33 eV) and a laser beam spot size of ∼0.7 μm. The morphology and other features obtained from the μ-Raman spectroscopy study of $CsPbCl_3$ NWs are shown in Figure 3. The optical image and

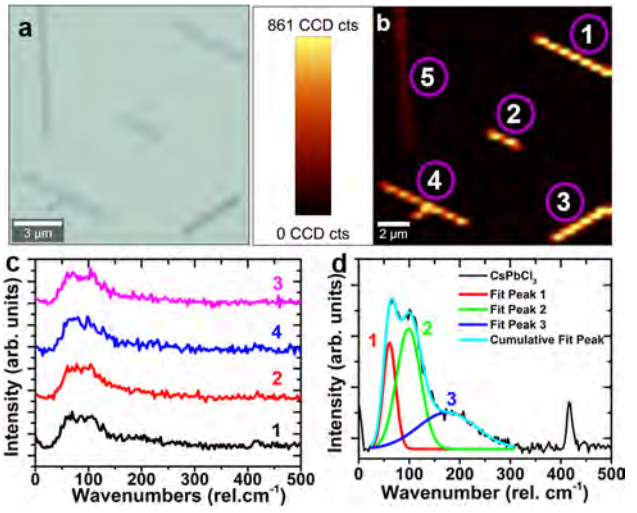

Figure 3. μ-Raman mapping of AIHP $CsPbCl_3$ NWs grown on the c-Al_2O_3 substrate. (a) Confocal optical microscopy image and (b) the corresponding μ-Raman mapping of $CsPbCl_3$ NWs. (c) Raman spectra of four (4) different NWs. (d) Fitted Raman spectrum of $CsPbCl_3$ NWs showing the three TO phonon modes of $CsPbCl_3$. No spectral shift is observed for any of the all-inorganic $CsPbCl_3$ halide perovskite NW structures under investigation showing their crystalline homogeneity.

the corresponding μ-Raman scan are shown, respectively, in Figure 3a,b, while the μ-Raman peaks obtained for four different NWs are presented in Figure 3c. Raman signatures obtained for different NWs falling in the range of 50−250 cm^{-1} are similar and are also in good agreement with that reported for $CsPbCl_3$ nanocrystals by Liao et al.[42] The similarity of the Raman signatures observed for the 4 different NWs (Figure 3c) further confirms that the NWs are of the same perovskite crystal structure. The Raman spectrum of a randomly selected NW can be fitted with three transverse optical (TO) mode phonon peaks, as shown in Figure 3d. We note that the three phonon peaks found, respectively, at around 61, 98, and 174 cm^{-1} are common to all 4 different

https://doi.org/10.1021/acsanm.5c04170
ACS Appl. Nano Mater. 2025, 8, 23933−23944

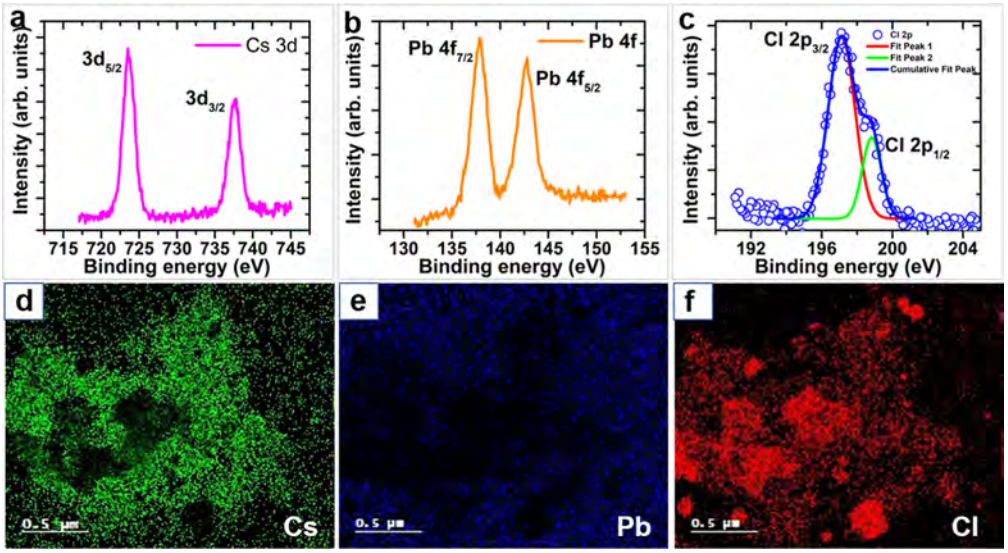

Figure 4. XPS and energy-dispersive X-ray spectroscopy (EDS) measurements for composition analyses of $CsPbCl_3$ NWs. High-resolution XPS core level spectra of (a) Cs 3d; (b) Pb 4f; and (c) Cl 2p obtained for $CsPbCl_3$ NWs. (d–f) Energy-dispersive X-ray spectroscopy (EDS) maps of Cs, Pb, and Cl showing the distribution of the elements in the $CsPbCl_3$ NW structures drop-casted on the C-coated Cu grid. Maps were taken in an EDS system coupled with the STEM facility.

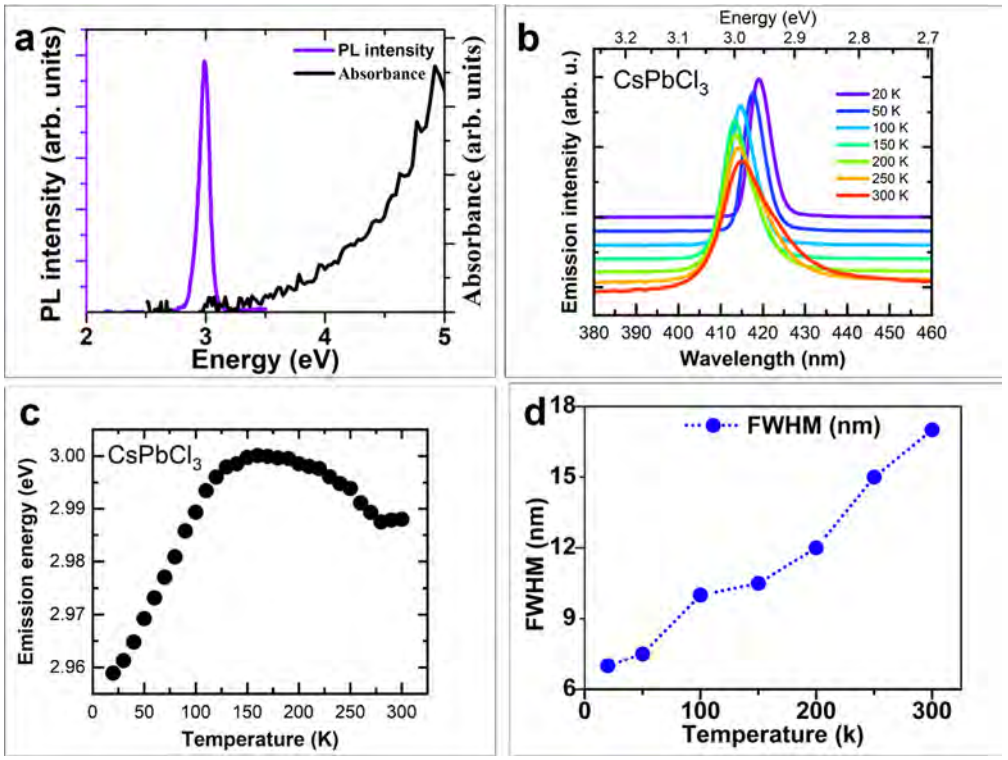

Figure 5. Steady-state and temperature-dependent PL studies of NC–CVD-grown self-assembled $CsPbCl_3$ NWs. (a) Steady-state PL emission and absorption spectra. (b) Temperature-dependent PL emissions measured in the range of (15–300) K. (c) PL emission energy vs temperature and (d) temperature dependency of the PL-fwhm.

NWs under observation and are in good agreement with literature data obtained for the nanocrystals and single-crystal ingots of the same material.[42,43] The peak observed at around 417 cm^{-1} corresponds to the Raman shift from the c-Al_2O_3 substrate.

3.2. Composition Analysis. X-ray photoelectron spectroscopy (XPS) measurements were performed to determine the elemental composition and valence state of different elements in the $CsPbCl_3$ NWs. The C 1s peak at 284.14 eV was used as the energy calibration for the binding energies in the XPS core level spectra. The core level spectra of Cs 3d, Pb 4f, and Cl 2p of the $CsPbCl_3$ NWs are shown in Figure 4a–c. The Cs $3d_{5/2}$ and Cs $3d_{3/2}$ peaks with binding energies, respectively, at 723.6 and 737.59 eV exhibited in Figure 4a are comparable to those obtained for the $CsPbCl_3$ quantum dots, nanocrystals, and other structures reported in the litera-

https://doi.org/10.1021/acsanm.5c04170
ACS Appl. Nano Mater. 2025, 8, 23933–23944

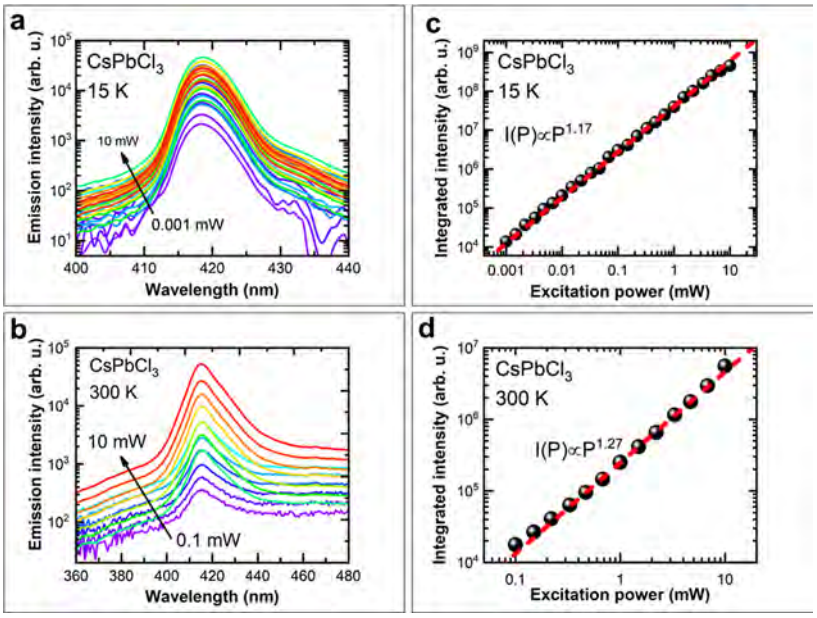

Figure 6. Power-dependent PL spectra of $CsPbCl_3$ NWs obtained for two different temperatures (a) 15 K and (b) 300 K, measured in the excitation power ranges of 0.001−10 mW and 0.1−10 mW, respectively. PL peak intensity as a function of the excitation power measured at (c) 15 K and (d) 300 K.

ture.[44−46] The observed peaks with binding energy values of 137.86 and 142.7 eV in Figure 4b are consistent with the binding energy values of Pb $4f_{7/2}$ and Pb $4f_{5/2}$, respectively, reported for $CsPbCl_3$ nanocrystals.[44,47] Moreover, the Cl $2p_{3/2}$ and Cl $2p_{1/2}$ core level peaks with respective binding energies of 197.4 and 199.5 eV shown in Figure 4c are also consistent with their literature reported values for $CsPbCl_3$ quantum dots and nanocrystals.[46,48] The atomic ratio obtained from the XPS measurements of $CsPbCl_3$ NWs is Cs/Pb/Cl = 24.4:23.6:52.0, which closely matches the basic halide perovskite composition ratio of 1:1:3. Composition information obtained from XPS measurements was further confirmed by energy-dispersive X-ray spectroscopy (EDS) in the scanning TEM (STEM). EDS elemental mappings of $CsPbCl_3$ nanowires reveal that all of the elements are distributed evenly throughout the sample. The elemental maps of the sonicated $CsPbCl_3$ NW structures are shown in Figure 4d−f.

3.3. Optical Properties of $CsPbCl_3$ NWs. Photoluminescence (PL) properties of the AIHP $CsPbCl_3$ NWs were studied by using a home-built PL setup with a 325 nm He−Cd laser as the excitation source performed at room temperature. Figure 5a reveals that $CsPbCl_3$ NWs exhibit strong violet-blue (∼415 nm (∼2.99 eV)) emission. The PL peak is relatively sharp with a full width at half-maximum (fwhm) value of 14 nm which is narrower than those reported for colloidal nanocrystals,[49] micro/nanorods,[4] and microplates[50] and therefore suggests that $CsPbCl_3$ NWs grown by the NC−CVD process have high crystalline quality. To relate the absorption edge with the PL emission peak, we performed spectrophotometry measurements on the $CsPbCl_3$ NWs in the spectral range of 200 to 1700 nm. The absorbance spectrum plotted together with the PL spectrum shown in Figure 5a shows that the PL peak energy is close to the absorption edge for $CsPbCl_3$ NWs, which suggests that the emission is a band-edge-related emission, and the estimated bandgap E_g is at ∼2.99 eV. The character of this emission is excitonic, which is confirmed by PL measurements as a function of excitation intensity presented later. Note that we could not obtain the absolute absorbance of the AIHP ternary $CsPbCl_3$ NWs since the probe beam size (2 mm) was much larger than the NW structures, so that a large portion of the beam passes through areas with no deposited structures. Moreover, the beam covered several NWs with slightly different thicknesses. Hence, the appearance of the absorption spectrum in Figure 5a is different from that obtained from a uniform thin film sample.

In most conventional III−V and II−VI semiconductors, the bandgap decreases with the increase in temperature, so that their PL peaks are red-shifted. However, for the $CsPbCl_3$ NWs, we observe an anomalous temperature-dependent PL emission behavior, i.e., the emission peak shifts to higher energy as the temperature increases. Figure 5b shows the temperature-dependent PL measurements of $CsPbCl_3$ NWs from 20 to 300 K. The PL peak energy increases as the temperature increases from 20 K (2.96 eV) and reaches a maximum value of 3.01 eV at 200 K. At temperatures higher than 200 K, the PL peak energy gradually drops to ∼2.99 eV at 300 K. The temperature dependency of the energy of the PL peak is summarized in Figure 5c. A very similar blue shift followed by a red shift in the PL emission features for $CsPbCl_3$ nanowires and nanocrystals were also reported, respectively, by Gao et al. and Lohar et al.[51,52]

They attributed this shifting in the PL peaks to the nature of the valence band maximum states of the $CsPbCl_3$ perovskite which came from the hybridization of the 3p orbitals of the Cl atom with the 6s orbitals of the Pb.[4,51] Due to lattice thermal shrinkage, the contact between two orbitals increases as the temperature drops; as a result, the band gap narrows, and the emission peak red shifts. Meanwhile, electron−phonon scattering is reduced with decreasing temperature, which causes the emission peak to blue shift.[51] In addition to the blue shift in the PL peak, as shown in Figure 5b,c, with increasing temperature, the peak also broadens with a decrease in the peak intensity (Figure 5d). This drop in the PL intensity is similar to that reported for the $CsPbCl_3$ nanocrystals by Lohar

https://doi.org/10.1021/acsanm.5c04170
ACS Appl. Nano Mater. 2025, 8, 23933−23944

et al. where they attributed it to be caused by the defect-related transitions.[52] Previous reports on PL emissions from ultrathin $CsPbCl_3$ NWs and $CsPbCl_3$ NCs were suggested to arise from free excitonic/excitonic emissions originated from exciton−phonon or electron−phonon interactions.[8,51−53] Since similar PL emissions are observed from our $CsPbCl_3$ NWs, they may also be attributed to mechanisms suggested by these earlier reports.

Nevertheless, $CsPbX_3$ (X = Cl, Br, and I) perovskites are observed to have a cubic phase at high temperature and transform to other stable phases at the room temperature.[50,54] More specifically, $CsPbCl_3$ was reported to have a cubic phase at temperatures ≥47 °C[54−56] and transformed to stable tetragonal (nano)[40] and monoclinic (bulk)[50] phases at room temperature. It was also reported that $CsPbCl_3$ may exist in multiple phases within a limited temperature range of 310 to 320 K.[52] However, since our temperature-dependent PL studies were confined to the temperature range between 20 and 300 K, phase transition and/or the presence of multiple phases within this temperature range and hence the PL peak shifts due to phase transition are therefore not expected here for the $CsPbCl_3$ NWs. In addition, the defect-related emissions spectrum usually appears in the longer wavelength region than the band edge emission spectrum. As shown in Figure 5a, the steady-state room temperature PL from $CsPbCl_3$ NWs appeared at ∼415 nm. Since the temperature-dependent PL data (Figure 5b,c) we obtained only deviates by ∼5 nm from the fundamental one, we believe that the observed continuous PL peak shifting is not caused by defect-related emission as well.

In order to understand the origin of the photophysics of the $CsPbCl_3$ NWs, we also performed power-dependent PL studies. Figure 6a,b, respectively, show the PL peak intensity from $CsPbCl_3$ NWs measured at 15 and 300 K with increasing excitation power, 0.001−10 mW (15 K) and 0.1−10 mW (300 K). No noticeable shift or broadening of the PL peak is observed as the excitation power increases over several orders of magnitude. The integrated PL peak intensity as a function of the excitation power obtained for 15 and 300 K are depicted in Figure 6c,d, respectively. As per the power law fitting, $I \propto P_{ex}^{\alpha}$, the value of α falls between 1 and 2 for both temperatures. This suggests that the PL emission from the $CsPbCl_3$ NWs arises from the free- or bound-exciton transitions.[51,57] However, in order to have a detailed understanding of the true excitonic nature and to clarify if the luminescence is governed by free excitons or bound excitons transitions, further studies are required.

3.4. $CsPbCl_3$ NWs as Multiphoton Absorbing NLO Materials. Multiphoton absorption (MPA) is a NLO phenomenon that involves the simultaneous absorption of a greater number (more than two) of NIR photons followed by the subsequent nonradiative and radiative recombination and thereby the emission of a shorter wavelength photon.[21,31] To study the prospect of the NC−CVD-grown AIHP $CsPbCl_3$ NWs as the NLO material, here, we performed one-, two-, and three- photon (1P-, 2P-, and 3P-) pumped PL studies. A laser scanning confocal multiphoton microscope (Leica TCS SP8) equipped with a Ti:Sapphire femtosecond laser (Spectra-physics, Ma Tai HP; pulse duration: 100 fs; and repetition rate: 80 MHz) was used for the MPA PL measurements of $CsPbCl_3$ NWs. The emission spectra were collected accordingly from the integrated hybrid detection unit coupled to the microscopy setup. Figure 7a shows the 1-(λ_{exc} = 320 nm), 2-(λ_{exc} = 800 nm), and 3-photon (λ_{exc} = 900 nm) pumped PL spectra from $CsPbCl_3$ NWs with PL peaks centered at 416, 426, and 422 nm, respectively. These slight red shifts in multiphoton excited PL peaks are commonly observed in NLO materials and can be attributed to the increased reabsorption effects experienced due to the larger penetration depth caused by the longer wavelength TP/MP excitations.[58−61] Because the emitted photons come from deeper regions, they undergo multiple reabsorption and re-emission cycles, and the PL peak may be red-shifted due to energy loss to phonons or nonradiative relaxation in each cycle. A schematic of the 3-photon absorption and the corresponding PL emission and SHG mechanisms under 900 nm excitation is presented in Figure 7b. Figure 7c shows the three-photon excited PL peak of the $CsPbCl_3$ NWs fitted with two peaks centered, respectively, at ∼423 and ∼450 nm (referred to as peaks 1 and 2, respectively). Peak 1 centered at ∼423 nm is very close to the fundamental emission wavelength of $CsPbCl_3$, while Peak 2 centered at ∼450 nm corresponds to the SH of the excitation wavelength, λ_{exc} = 900 nm. Excitation power-dependent three-photon excited PL spectra of $CsPbCl_3$ NWs are shown in Figure 7d. At lower excitation power, only the SH peak is found to be dominating. However, with the increase in the excitation power, the intensity of the fundamental emissions from the $CsPbCl_3$ NWs at ∼423 nm becomes the dominating feature in the spectra and increases in a superlinear way. In contrast, since the SH peak arises from the surface and quickly saturates, its intensity remains relatively constant in response to the increased excitation powers. All these observations clearly suggest that $CsPbCl_3$ NWs have high prospects as active NLO components in the miniaturized integrated photonic and optoelectronic devices.

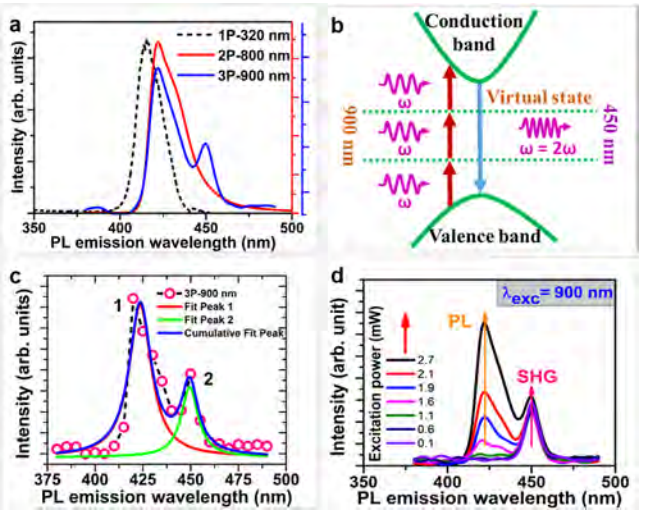

Figure 7. Multiphoton absorption (MPA) in $CsPbCl_3$ NWs. (a) One (1)-, Two (2)-, and Three (3)-photon excited PL emission spectra of self-assembled $CsPbCl_3$ NWs and (b) a schematic diagram showing the 3-photon absorption, PL emission, and SH generation processes. (c) Three (3)-photon (900 nm) excited PL spectrum of $CsPbCl_3$ NWs fitted with two peaks centered, respectively, at ∼423 nm (PL emission) and ∼450 nm (second harmonic generation (SHG)). (d) Excitation power dependency of the three (3)-photon excited PL and SHG spectra of $CsPbCl_3$ NWs.

3.5. $CsPbCl_3$ NWs as a High-*Q* Cavity Resonator. It has been established that AIHPs materials have excellent intrinsic lasing properties and that their triangular prismatic-shaped NW

https://doi.org/10.1021/acsanm.5c04170
ACS Appl. Nano Mater. 2025, 8, 23933−23944

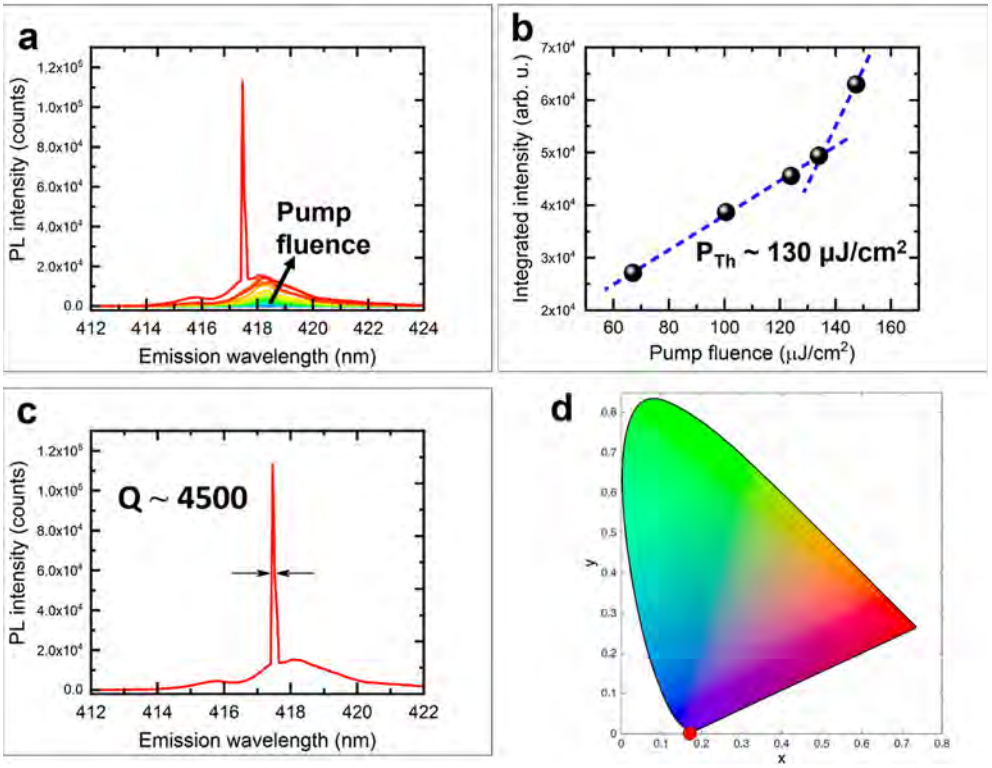

Figure 8. Single-mode lasing and the CIE plot for typical $CsPbCl_3$ NW. (a) Pumping fluence-dependent PL spectra of self-assembled all-inorganic $CsPbCl_3$ NW measured at 4.7 K, grown by the NC−CVD approach. (b) Nonlinear response of the PL intensity curve. (c) Single-mode lasing emission spectrum realized at $P_{Th} \sim 130\ \mu J/cm^2$ and the quality factor (Q) of the resonator cavity, and (d) the CIE plot with the PL emission from the $CsPbCl_3$ NW.

Table 1. Quality Factor (Q) Values of Various Morphologies of the $CsPbCl_3$ Perovskite

synthesis method	composition	morphology	measuring temp	P_{th}	Q	ref
solution	$CsPbCl_3$	NW	RT	~6 $\mu J/cm^2$	1300	14
solution	$CsPbCl_3$	NW	RT	~86 $\mu J/cm^2$	690	63
solution	$CsPbCl_3$	microplate	83 K	~25 mJ/cm^2	1400	64
CVT	$CsPbCl_3$	NW	RT	7 $\mu J/cm^2$	1400	65
CVD	$CsPbBr_3$	NR	RT	~14.1 $\mu J/cm^2$	3500	4
CVD	$CsPbI_3$	NW	RT	21 $\mu J/cm^2$	2256	66
CVD	$CsPbCl_3$	NW	RT	11 $\mu J/cm^2$	1931	66
NC−CVD	$CsPbCl_3$	NW	4.7 K	~130 $\mu J/cm^2$	~4500	this work

structures were well suited for miniaturized lasing applications.[4] Here, as depicted in Figure 7d, the excitation power dependency of the three-photon pumped PL spectra realized for the AIHP $CsPbCl_3$ NWs further shed light on their prospect for lasing like NLO applications. To explore the prospects of the NWs for lasing applications, fluence-dependent PL properties were measured for a typical $CsPbCl_3$ NW sample at 4.7 K under a frequency-doubled 380 nm excitation, and the results are shown in Figure 8. As seen from Figure 8a, with an increase in the optical pumping fluence, the PL peak intensity increases gradually up to a threshold power of ~130 $\mu J/cm^2$ when a sharp resonance peak emerges. A nonlinear dependency of the PL intensity with the pumping fluence is clearly observed from the plot of the PL peak intensity with increasing pump power shown in Figure 8b. The observed sharp-intense PL emission centered at $\lambda \sim 417.46$ nm with an extremely narrow line width of $\delta\lambda \sim 0.091$ nm excited with a laser power density of ~130 $\mu J/cm^2$ results in a high-quality lasing cavity $Q = \frac{\lambda}{\delta\lambda}$ of ~4500. This is higher than most reported $CsPbCl_3$ cavities Q-value obtained for low- and room-temperature measured ASE/lasing. Note that Gradečak et al. carried out a comparative finite-difference time-domain (FDTD) analysis and demonstrated a higher Q value for triangular GaN nanowire than that of its near cylindrical geometric counterpart.[19] Also, it is reported that the optical scattering loss at the edge-substrate planar interface for a triangular NW cavity is significantly suppressed compared to that of the point interface for a cylindrical NW[62] and hence promote higher Q value. In our NC−CVD growth process, the high-temperature materials treatment facilitated the growth of triangular geometric semiconducting nanowires.[4] Moreover, compared to other traditional vapor growths like catalytic-CVD, NC−CVD favors semiconductor nanostructures' growth with higher crystalline quality with low defect density.[4,5,41] Therefore, the high Q value obtained here for the $CsPbCl_3$ NW cavity resonator can be attributed to its high-quality single-crystalline triangular geometry obtained from NC−CVD growth. Table 1 compares the "Q" value obtained in this work with reported Q values for various $CsPbCl_3$/AIHP morphol-

https://doi.org/10.1021/acsanm.5c04170
ACS Appl. Nano Mater. 2025, 8, 23933−23944

ogies measured at low to room temperatures and under one- and multiphoton excitations.

We note that lasing from our $CsPbCl_3$ NWs was not realized at room temperature. We believe that although $CsPbX_3$ has a high exciton binding energy (~30−80 meV), at room temperature, they dissociate into free carriers because of thermal fluctuations. Therefore, at RT, instead of excitonic emissions, photoexcited band to band emissions occur due to free carrier recombination, which, however, has a larger optical loss than that caused by the excitonic emissions. This suppresses the ASE and thus the lasing from the $CsPbX_3$ cavities during the room temperature measurements.[35,67] Also, we suspect that the surface degradation of the sample might also contribute to the absence of the room temperature lasing since the $CsPbCl_3$ NW samples were kept in a drybox for over a year before the ASE/lasing setup was available for our measurements. However, it is possible that such surface degradation can be overcome via physical or chemical passivation processes[68] and thus realize room temperature lasing. Therefore, in addition to surface passivation, avoidance of material aging should also be taken into account in the future to achieve room temperature lasing from these types of halide NWs. In addition, another possible reason may lie in the chloride vacancy-related trap states within the bandgap of $CsPbCl_3$ which may escalate nonradiative recombination and thereby results in a sharp reduction in the PLQY. Consequently, this may increase the lasing threshold value and hinder the appearance of the room temperature ASE in $CsPbCl_3$ nanowires.[20,34,69,70] Moreover, the smaller modal volume of the cavity may also be responsible for the increased lasing threshold of these NWs.[34,38] Nevertheless, the nonlinear PL intensity response shown in Figure 8b demonstrates lasing generation in the NW cavity with a threshold value of ~130 $\mu J/cm^2$, which is relatively high for such systems, probably due to the surface degradation of the NW sample. The single-mode lasing spectrum shown in Figure 8c can be attributed to the one-dimensional triangular morphology of the $CsPbCl_3$ NW cavity along with its high-quality singe-crystalline nature. Here, we note the FDTD study of the electric field intensity distribution in NWs with triangular cross-section by Zhou et al. which demonstrated that single-mode lasing occurs in this type of nanowires.[4] Furthermore, the triangular geometry-induced intrinsic excellent optical field confinement[7,31] along with extremely narrow gain region offered by the distinctive size of the nanowire as nanocavity resonator[22,39] could also promote the observed single-mode lasing in $CsPbCl_3$ NWs. These optical properties confirm that $CsPbCl_3$ NWs have high potential for cavity as well as gain medium applications. Moreover, the Commission Internationale de L'Eclairage (CIE) chromaticity plot obtained for the emission spectrum in Figure 8c is shown in Figure 8d. It is seen that the PL emission from the $CsPbCl_3$ NW at ~415 nm is located at the bottom of the CIE diagram. The blue emission from the NC−CVD grown self-assembled AIHP $CsPbCl_3$ NWs further demonstrates their prospect for future color display device applications.

4. CONCLUSIONS

In this work, we report on the emission properties of $CsPbCl_3$ nanowires with particular emphasis on the SHG and lasing with a high quality factor. Our results suggest that these $CsPbCl_3$ NWs are single-crystalline with a high crystalline quality. The narrow, intense violet-blue (~415 nm) PL emission, excellent response to the two- and multiphoton absorption-related excitations along with SHG from these $CsPbCl_3$ NWs show their prospects for various light generation and manipulation applications, namely, miniaturized color display devices and lasers, fluorescence imaging, multiphoton microscopy, biological imaging, photodynamic therapy, laser tomography, and so on. Also, both temperature- and power-dependent PL measurements verify that the PL emissions from the $CsPbCl_3$ NWs originate from excitonic transitions. Excellent lasing with a single-mode lasing spectrum is also realized at a lasing threshold ~130 $\mu J/cm^2$. The narrow line width of the lasing spectrum ($\delta\lambda \sim 0.091$ nm) enables the nanocavity to achieve a quality factor value of $Q \sim 4500$, much higher than most reported values on this material with different structures, dimensions, and measurement temperature. We believe that these findings advance and promote the one- and multiphoton absorption-related cavity and gain medium applications of $CsPbX_3$ (X = Cl, Br, and I) perovskites and their miniaturizations as well. The insights of the photophysical transition mechanism disclosed here for $CsPbCl_3$ NWs may also be relevant to enhance the understanding of the photophysics of other wide bandgap semiconductors.

■ ASSOCIATED CONTENT

Data Availability Statement

Data are available from the corresponding authors only upon request.

Supporting Information

The Supporting Information is available free of charge at https://pubs.acs.org/doi/10.1021/acsanm.5c04170.

Additional information on materials characterization; surface guiding and grapho-epitaxial effect in $CsPbCl_3$ NWs growth; and surface guiding and grapho-epitaxial effect (PDF)

■ AUTHOR INFORMATION

Corresponding Authors

Mohammad Kamal Hossain − *Department of Physics, Comilla University, Cumilla 3506, Bangladesh; Department of Physics, City University of Hong Kong, Kowloon 999077, Hong Kong;* orcid.org/0000-0002-9902-834X; Email: kamal.phys@cou.ac.bd

Kin Man Yu − *Department of Physics, City University of Hong Kong, Kowloon 999077, Hong Kong; Department of Physics, National Sun Yat-sen University, Kaohsiung 80424, Taiwan;* orcid.org/0000-0003-1350-9642; Email: kinmanyu@cityu.edu.hk

Authors

Szymon J. Zelewski − *Department of Semiconductor Materials Engineering, Wroclaw University of Science and Technology, Wroclaw 50-370, Poland;* orcid.org/0000-0002-6037-3701

Robert Kudrawiec − *Department of Semiconductor Materials Engineering, Wroclaw University of Science and Technology, Wroclaw 50-370, Poland;* orcid.org/0000-0003-2593-9172

Marcin Syperek − *Department of Experimental Physics, Wroclaw University of Science and Technology, Wroclaw 50-370, Poland;* orcid.org/0000-0002-5260-7360

Roberto dos. Reis − *Northwestern University, Evanston, Illinois 60208, United States*

https://doi.org/10.1021/acsanm.5c04170
ACS Appl. Nano Mater. 2025, 8, 23933−23944

Yuen Hong Tsang − *Department of Applied Physics, The Hong Kong Polytechnic University, Kowloon 999077, Hong Kong;* orcid.org/0000-0001-5632-5224

Johnny C. Ho − *Department of Materials Science and Engineering, City University of Hong Kong, Kowloon 999077, Hong Kong;* orcid.org/0000-0003-3000-8794

Complete contact information is available at: https://pubs.acs.org/10.1021/acsanm.5c04170

Notes

The authors declare no competing financial interest.

■ ACKNOWLEDGMENTS

This work was supported by CityU SGP (no. 9380076).

■ REFERENCES

(1) Zheng, X.; Hou, Y.; Bao, C.; Yin, J.; Yuan, F.; Huang, Z.; Song, K.; Liu, J.; Troughton, J.; Gasparini, N.; Zhou, C.; Lin, Y.; Xue, D. J.; Chen, B.; Johnston, A. K.; Wei, N.; Hedhili, M. N.; Wei, M.; Alsalloum, A. Y.; Maity, P.; Turedi, B.; Yang, C.; Baran, D.; Anthopoulos, T. D.; Han, Y.; Lu, Z. H.; Mohammed, O. F.; Gao, F.; Sargent, E. H.; Bakr, O. M. Managing Grains and Interfaces via Ligand Anchoring Enables 22.3%-Efficiency Inverted Perovskite Solar Cells. *Nat. Energy* **2020**, *5* (2), 131−140.

(2) https://www.nrel.gov/pv/assets/pdfs/best-research-cell-efficiencies.pdf,BestResearch-CellEfficiencies,NREL (accessed Sep 09, 2025).

(3) Lai, M.; Kong, Q.; Bischak, C. G.; Yu, Y.; Dou, L.; Eaton, S. W.; Ginsberg, N. S.; Yang, P. Structural, Optical, and Electrical Properties of Phase-Controlled Cesium Lead Iodide Nanowires. *Nano Res.* **2017**, *10* (4), 1107−1114.

(4) Zhou, H.; Yuan, S.; Wang, X.; Xu, T.; Wang, X.; Li, H.; Zheng, W.; Fan, P.; Li, Y.; Sun, L.; Pan, A. Vapor Growth and Tunable Lasing of Band Gap Engineered Cesium Lead Halide Perovskite Micro/Nanorods with Triangular Cross Section. *ACS Nano* **2017**, *11* (2), 1189−1195.

(5) Chen, J.; Fu, Y.; Samad, L.; Dang, L.; Zhao, Y.; Shen, S.; Guo, L.; Jin, S. Vapor-Phase Epitaxial Growth of Aligned Nanowire Networks of Cesium Lead Halide Perovskites ($CsPbX_3$, X = Cl, Br, I). *Nano Lett.* **2017**, *17* (1), 460−466.

(6) Gui, P.; Chen, Z.; Li, B.; Yao, F.; Zheng, X.; Lin, Q.; Fang, G. High-Performance Photodetectors Based on Single All-Inorganic $CsPbBr_3$ Perovskite Microwire. *ACS Photonics* **2018**, *5* (6), 2113−2119.

(7) Wang, Y.; Sun, X.; Shivanna, R.; Yang, Y.; Chen, Z.; Guo, Y.; Wang, G. C.; Wertz, E.; Deschler, F.; Cai, Z.; Zhou, H.; Lu, T. M.; Shi, J. Photon Transport in One-Dimensional Incommensurately Epitaxial $CsPbX_3$ Arrays. *Nano Lett.* **2016**, *16* (12), 7974−7981.

(8) Gao, Y.; Zhao, L.; Shang, Q.; Zhong, Y.; Liu, Z.; Chen, J.; Zhang, Z.; Shi, J.; Du, W.; Zhang, Y.; Chen, S.; Gao, P.; Liu, X.; Wang, X.; Zhang, Q. Ultrathin $CsPbX_3$ Nanowire Arrays with Strong Emission Anisotropy. *Adv. Mater.* **2018**, *30* (31), 1−9.

(9) Zhang, D.; Eaton, S. W.; Yu, Y.; Dou, L.; Yang, P. Solution-Phase Synthesis of Cesium Lead Halide Perovskite Nanowires. *J. Am. Chem. Soc.* **2015**, *137* (29), 9230−9233.

(10) Ishii, A.; Miyasaka, T. Quantum Cutting-Induced near-Infrared Luminescence of $Yb^{3+}$and Er^{3+}in a Layer Structured Perovskite Film. *J. Chem. Phys.* **2020**, *153* (19), 194704.

(11) Fan, T.; Lü, J. t.; Deng, W.; Mai, J. x.; Liang, J.; Deng, T. t.; Fan, W.; Zhou, Q. s.; Lin, Q. f. Orange LED and Cell Fluorescence Imaging of Mn^{2+} Doped $CsPbCl_3$ Water-Soluble Nanocrystals with Improved Stability and Optimized Luminescence. *Ceram. Int.* **2023**, *49* (8), 13066−13073.

(12) Stefanski, M.; Bondzior, B.; Basinski, A.; Ptak, M.; Lou, B.; Ma, C. G. Synthesis and Characterization of a $CsPbCl_3$ Perovskite Doped with Nd^{3+}: Structural, Optical, and Energy Transfer Properties. *Inorg. Chem. Front.* **2024**, *11* (9), 2626−2633.

(13) Milstein, T. J.; Kroupa, D. M.; Gamelin, D. R. Picosecond Quantum Cutting Generates Photoluminescence Quantum Yields over 100% in Ytterbium-Doped $CsPbCl_3$ Nanocrystals. *Nano Lett.* **2018**, *18* (6), 3792−3799.

(14) Fu, Y.; Zhu, H.; Stoumpos, C. C.; Ding, Q.; Wang, J.; Kanatzidis, M. G.; Zhu, X.; Jin, S. Broad Wavelength Tunable Robust Lasing from Single-Crystal Nanowires of Cesium Lead Halide Perovskites ($CsPbX_3$, X = Cl, Br, I). *ACS Nano* **2016**, *10* (8), 7963−7972.

(15) Fu, Y.; Zhu, H.; Chen, J.; Hautzinger, M. P.; Zhu, X. Y.; Jin, S. Metal Halide Perovskite Nanostructures for Optoelectronic Applications and the Study of Physical Properties. *Nat. Rev. Mater.* **2019**, *4* (3), 169−188.

(16) Hong, K.; Van Le, Q.; Kim, S. Y.; Jang, H. W. Low-Dimensional Halide Perovskites: Review and Issues. *J. Mater. Chem. C* **2018**, *6* (9), 2189−2209.

(17) Li, X. L.; Chen, C.; Yang, Z. Y.; Meng, X. S.; Zhu, Y. B.; Feng, X. F.; Gao, Y. C.; Wang, W. Z.; Liu, J. W. Unique Nanowire Assemblies Enables Superior Anti-Interference Capability for Accurate Structural Failure Prediction and Soft Robotics. *Nano Res.* **2025**, *18* (7), 94906990.

(18) Meyers, J. K.; Kim, S.; Hill, D. J.; Cating, E. E. M.; Williams, L. J.; Kumbhar, A. S.; McBride, J. R.; Papanikolas, J. M.; Cahoon, J. F. Self-Catalyzed Vapor−Liquid−Solid Growth of Lead Halide Nanowires and Conversion to Hybrid Perovskites. *Nano Lett.* **2017**, *17* (12), 7561−7568.

(19) Gradečak, S.; Qian, F.; Li, Y.; Park, H. G.; Lieber, C. M. GaN Nanowire Lasers with Low Lasing Thresholds. *Appl. Phys. Lett.* **2005**, *87* (17), 1−3.

(20) Zhu, H.; Fu, Y.; Meng, F.; Wu, X.; Gong, Z.; Ding, Q.; Gustafsson, M. V.; Trinh, M. T.; Jin, S.; Zhu, X. Y. Lead Halide Perovskite Nanowire Lasers with Low Lasing Thresholds and High Quality Factors. *Nat. Mater.* **2015**, *14* (6), 636−642.

(21) Pramanik, A.; Gates, K.; Gao, Y.; Begum, S.; Chandra Ray, P. Several Orders-of-Magnitude Enhancement of Multiphoton Absorption Property for $CsPbX_3$ Perovskite Quantum Dots by Manipulating Halide Stoichiometry. *J. Phys. Chem. C* **2019**, *123* (8), 5150−5156.

(22) Huang, C.; Wang, K.; Yang, Z.; Jiang, L.; Liu, R.; Su, R.; Zhou, Z. K.; Wang, X. Up-Conversion Perovskite Nanolaser with Single Mode and Low Threshold. *J. Phys. Chem. C* **2017**, *121* (18), 10071−10077.

(23) Zhang, Z. Y.; Wang, H. Y.; Zhang, Y. X.; Li, K. J.; Zhan, X. P.; Gao, B. R.; Chen, Q. D.; Sun, H. B. Size-Dependent One-Photon- and Two-Photon-Pumped Amplified Spontaneous Emission from Organometal Halide $CH_3NH_3PbBr_3$ Perovskite Cubic Microcrystals. *Phys. Chem. Chem. Phys.* **2017**, *19* (3), 2217−2224.

(24) Chen, A.; Zhu, H.; Wu, Y.; Yang, D.; Li, J.; Yu, S.; Chen, Z.; Ren, Y.; Gui, X.; Wang, S.; Tang, Z. Low-Threshold Whispering-Gallery Mode Upconversion Lasing via Simultaneous Six-Photon Absorption. *Adv. Opt. Mater.* **2018**, *6* (17), 1−6.

(25) Fiebig, M.; Pavlov, V. V.; Pisarev, R. V. Second-Harmonic Generation as a Tool for Studying Electronic and Magnetic Structures of Crystals: Review. *J. Opt. Soc. Am. B* **2005**, *22* (1), 96.

(26) Saouma, F. O.; Stoumpos, C. C.; Kanatzidis, M. G.; Kim, Y. S.; Jang, J. I. Multiphoton Absorption Order of $CsPbBr_3$ as Determined by Wavelength-Dependent Nonlinear Optical Spectroscopy. *J. Phys. Chem. Lett.* **2017**, *8* (19), 4912−4917.

(27) Saouma, F. O.; Park, D. Y.; Kim, S. H.; Jeong, M. S.; Jang, J. I. Multiphoton Absorption Coefficients of Organic-Inorganic Lead Halide Perovskites $CH_3NH_3PbX_3$ (X = Cl, Br, I) Single Crystals. *Chem. Mater.* **2017**, *29* (16), 6876−6882.

(28) Walters, G.; Sutherland, B. R.; Hoogland, S.; Shi, D.; Comin, R.; Sellan, D. P.; Bakr, O. M.; Sargent, E. H. Two-Photon Absorption in Organometallic Bromide Perovskites. *ACS Nano* **2015**, *9* (9), 9340−9346.

(29) He, T.; Li, J.; Qiu, X.; Xiao, S.; Yin, C.; Lin, X. Highly Enhanced Normalized-Volume Multiphoton Absorption in $CsPbBr_3$ 2D Nanoplates. *Adv. Opt. Mater.* **2018**, *6* (21), 2−8.

(30) He, H.; Ma, E.; Chen, X.; Yang, D.; Chen, B.; Qian, G. Single Crystal Perovskite Microplate for High-Order Multiphoton Excitation. *Small Methods* **2019**, *3* (12), 1−7.
(31) Wang, X.; Zhou, H.; Yuan, S.; Zheng, W.; Jiang, Y.; Zhuang, X.; Liu, H.; Zhang, Q.; Zhu, X.; Wang, X.; et al. Cesium Lead Halide Perovskite Triangular Nanorods as High-Gain Medium and Effective Cavities for Multiphoton- Pumped Lasing. *Nano Res.* **2017**, *10* (10), 3385−3395.
(32) Moffatt, J. E.; Tsiminis, G.; Klantsataya, E.; de Prinse, T. J.; Ottaway, D.; Spooner, N. A. A Practical Review of Shorter than Excitation Wavelength Light Emission Processes. *Appl. Spectrosc. Rev.* **2020**, *55* (4), 327−349.
(33) Abdelwahab, I.; Grinblat, G.; Leng, K.; Li, Y.; Chi, X.; Rusydi, A.; Maier, S. A.; Loh, K. P. Highly Enhanced Third-Harmonic Generation in 2D Perovskites at Excitonic Resonances. *ACS Nano* **2018**, *12* (1), 644−650.
(34) Pina, J. M.; Parmar, D. H.; Bappi, G.; Zhou, C.; Choubisa, H.; Vafaie, M.; Najarian, A. M.; Bertens, K.; Sagar, L. K.; Dong, Y.; Gao, Y.; Hoogland, S.; Saidaminov, M. I.; Sargent, E. H. Deep-Blue Perovskite Single-Mode Lasing through Efficient Vapor-Assisted Chlorination. *Adv. Mater.* **2021**, *33* (5), 1−7.
(35) Zhang, Q.; Su, R.; Liu, X.; Xing, J.; Sum, T. C.; Xiong, Q. High-Quality Whispering-Gallery-Mode Lasing from Cesium Lead Halide Perovskite Nanoplatelets. *Adv. Funct. Mater.* **2016**, *26* (34), 6238−6245.
(36) Vahala, K. J. Optical Microcavities. In *2005 Eur. Quantum Electron. Conf. EQEC '05 2005*; IEEE, 2005.
(37) Guo, P.; Liu, D.; Shen, X.; Lv, Q.; Wu, Y.; Yang, Q.; Li, P.; Hao, Y.; Ho, J. C.; Yu, K. M. On-Wire Axial Perovskite Heterostructures for Monolithic Dual-Wavelength Laser. *Nano Energy* **2022**, *92* (November 2021), 106778.
(38) Guo, P.; Yang, Q.; Shen, X.; Lv, Q.; Hao, Y.; Xiao, L.; Ho, J. C.; Yu, K. M. Room-Temperature Broad-Wavelength-Tunable Single-Mode Lasing from Alloyed $CdS_{1-x}Se_x$ Nanotripods. *ACS Nano* **2022**, *16* (8), 12767−12776.
(39) Liu, S.; Sun, W.; Gu, Z.; Wang, K.; Zhang, N.; Xiao, S.; Song, Q. Tailoring the Lasing Modes in $CH_3NH_3PbBr_3$ Perovskite Microplates via Micro-Manipulation. *RSC Adv.* **2016**, *6* (56), 50553−50558.
(40) Hossain, M. K.; dos Reis, R.; Qarony, W.; Tsang, Y. H.; Ho, J. C.; Yu, K. M. Mechanism of Non-Catalytic Chemical Vapor Deposition Growth of All-Inorganic $CsPbX_3$(X = Br, Cl) Nanowires. *J. Mater. Chem. C* **2021**, *9* (9), 3229−3238.
(41) Shoaib, M.; Wang, X.; Zhang, X.; Wang, X.; Zhou, H.; Xu, T.; Hu, X.; Liu, H.; Fan, X.; Zheng, W.; Yang, T.; Yang, S.; Zhang, Q.; Zhu, X.; Sun, L.; Pan, A. Directional Growth of Ultralong $CsPbBr_3$ Perovskite Nanowires for High-Performance Photodetectors. *J. Am. Chem. Soc.* **2017**, *139* (44), 15592−15595.
(42) Liao, M.; Shan, B.; Li, M. In Situ Raman Spectroscopic Studies of Thermal Stability of All-Inorganic Cesium Lead Halide ($CsPbX_3$, X = Cl, Br, I) Perovskite Nanocrystals. *J. Phys. Chem. Lett.* **2019**, *10* (6), 1217−1225.
(43) Calistru, D. M.; Mihut, L.; Lefrant, S.; Baltog, I. Identification of the Symmetry of Phonon Modes in $CsPbCl_3$ in Phase IV by Raman and Resonance-Raman Scattering. *J. Appl. Phys.* **1997**, *82* (11), 5391−5395.
(44) Zhai, Y.; Bai, X.; Pan, G.; Zhu, J.; Shao, H.; Dong, B.; Xu, L.; Song, H. Effective Blue-Violet Photoluminescence through Lanthanum and Fluorine Ions Co-Doping for $CsPbCl_3$ Perovskite Quantum Dots. *Nanoscale* **2019**, *11* (5), 2484−2491.
(45) Ahmed, G. H.; El-Demellawi, J. K.; Yin, J.; Pan, J.; Velusamy, D. B.; Hedhili, M. N.; Alarousu, E.; Bakr, O. M.; Alshareef, H. N.; Mohammed, O. F. Giant Photoluminescence Enhancement in $CsPbCl_3$ Perovskite Nanocrystals by Simultaneous Dual-Surface Passivation. *ACS Energy Lett.* **2018**, *3* (10), 2301−2307.
(46) Liu, Y.; Pan, G.; Wang, R.; Shao, H.; Wang, H.; Xu, W.; Cui, H.; Song, H. Considerably Enhanced Exciton Emission of $CsPbCl_3$ Perovskite Quantum Dots by the Introduction of Potassium and Lanthanide Ions. *Nanoscale* **2018**, *10* (29), 14067−14072.
(47) Jiang, J.; Jin, Z.; Gao, F.; Sun, J.; Wang, Q.; Liu, S. (Frank). $CsPbCl_3$-Driven Low-Trap-Density Perovskite Grain Growth for > 20% Solar Cell Efficiency. *Adv. Sci.* **2018**, *5* (7), 1−7.
(48) Zhang, X.; Zhang, Y.; Zhang, X.; Yin, W.; Wang, Y.; Wang, H.; Lu, M.; Li, Z.; Gu, Z.; Yu, W. W. Yb^{3+} and Yb^{3+}/Er^{3+} Doping for near-Infrared Emission and Improved Stability of $CsPbCl_3$ Nanocrystals. *J. Mater. Chem. C* **2018**, *6* (37), 10101−10105.
(49) Yakunin, S.; Protesescu, L.; Krieg, F.; Bodnarchuk, M. I.; Nedelcu, G.; Humer, M.; De Luca, G.; Fiebig, M.; Heiss, W.; Kovalenko, M. V. Low-Threshold Amplified Spontaneous Emission and Lasing from Colloidal Nanocrystals of Caesium Lead Halide Perovskites. *Nat. Commun.* **2015**, *6*, 8056.
(50) Guo, P.; Hossain, M. K.; Shen, X.; Sun, H.; Yang, W.; Liu, C.; Ho, C. Y.; Kwok, C. K.; Tsang, S.; Luo, Y.; Ho, J. C.; Yu, K. M. Room-Temperature Red − Green − Blue Whispering-Gallery Mode Lasing and White-Light Emission from Cesium Lead Halide Perovskite ($CsPbX_3$, X = Cl, Br, I) Microstructures. *Adv. Opt. Mater.* **2018**, *6* (3), 1700993.
(51) Gao, Y.; Zhao, L.; Shang, Q.; Li, C.; Liu, Z.; Li, Q.; Wang, X.; Zhang, Q. Photoluminescence Properties of Ultrathin $CsPbCl_3$ Nanowires on Mica Substrate. *J. Semicond.* **2019**, *40* (5), 052201.
(52) Lohar, A. A.; Shinde, A.; Gahlaut, R.; Sagdeo, A.; Mahamuni, S. Enhanced Photoluminescence and Stimulated Emission in $CsPbCl_3$ Nanocrystals at Low Temperature. *J. Phys. Chem. C* **2018**, *122* (43), 25014−25020.
(53) Liu, Z.; Shang, Q.; Li, C.; Zhao, L.; Gao, Y.; Li, Q.; Chen, J.; Zhang, S.; Liu, X.; Fu, Y.; Zhang, Q. Temperature-Dependent Photoluminescence and Lasing Properties of $CsPbBr_3$ Nanowires. *Appl. Phys. Lett.* **2019**, *114* (10), 101902.
(54) Møller, C. K. Crystal Structure and Photoconductivity of Cæsium Plumbohalides. *Nature* **1958**, *182*, 1436.
(55) Wang, Y.; Guan, X.; Li, D.; Cheng, H.; Duan, X.; Lin, Z.; Duan, X. Chemical Vapor Deposition Growth of Single-Crystalline Cesium Lead Halide Microplatelets and Heterostructures for Optoelectronic Applications. *Nano Res.* **2017**, *10* (4), 1223−1233.
(56) Hossain, M. K.; Guo, P.; Qarony, W.; Tsang, Y. H.; Liu, C.; Tsang, S. W.; Ho, J. C.; Yu, K. M. Controllable Optical Emission Wavelength in All-Inorganic Halide Perovskite Alloy Microplates Grown by Two-Step Chemical Vapor Deposition. *Nano Res.* **2020**, *13* (11), 2939−2949.
(57) Schmidt, T.; Lischka, K.; Zulehner, W. Excitation-Power Dependence of the near-Band-Edge Photoluminescence of Semiconductors. *Phys. Rev. B* **1992**, *45* (16), 8989−8994.
(58) Gao, Y.; Wang, S.; Huang, C.; Yi, N.; Wang, K.; Xiao, S.; Song, Q. Room Temperature Three-Photon Pumped $CH_3NH_3PbBr_3$ Perovskite Microlasers. *Sci. Rep.* **2017**, *7*, 2−7.
(59) Zhao, C.; Tian, W.; Liu, J.; Sun, Q.; Luo, J.; Yuan, H.; Gai, B.; Tang, J.; Guo, J.; Jin, S. Stable Two-Photon Pumped Amplified Spontaneous Emission from Millimeter-Sized $CsPbBr_3$ Single Crystals. *J. Phys. Chem. Lett.* **2019**, *10*, 2357−2362.
(60) Xu, Y.; Chen, Q.; Zhang, C.; Wang, R.; Wu, H.; Zhang, X.; Xing, G.; Yu, W. W.; Wang, X.; Zhang, Y.; Xiao, M. Two-Photon-Pumped Perovskite Semiconductor Nanocrystal Lasers. *J. Am. Chem. Soc.* **2016**, *138* (11), 3761−3768.
(61) Yamada, Y.; Yamada, T.; Phuong, L. Q.; Maruyama, N.; Nishimura, H.; Wakamiya, A.; Murata, Y.; Kanemitsu, Y. Dynamic Optical Properties of $CH_3NH_3PbI_3$ Single Crystals As Revealed by One- and Two-Photon Excited Photoluminescence Measurements. *J. Am. Chem. Soc.* **2015**, *137* (33), 10456−10459.
(62) Zhang, Q.; Li, G.; Liu, X.; Qian, F.; Li, Y.; Sum, T. C.; Lieber, C. M.; Xiong, Q. A Room Temperature Low-Threshold Ultraviolet Plasmonic Nanolaser. *Nat. Commun.* **2014**, *5*, 1−9.
(63) Eaton, S. W.; Lai, M.; Gibson, N. A.; Wong, A. B.; Dou, L.; Ma, J.; Wang, L.-W.; Leone, S. R.; Yang, P. Lasing in Robust Cesium Lead Halide Perovskite Nanowires. *Proc. Natl. Acad. Sci. U.S.A.* **2016**, *113* (8), 1993−1998.
(64) Siu, C. K.; Zhao, J.; Wang, Y.; Yang, D.; Xu, X.; Pan, S.; Yu, S. F. Lasing Characteristics of Single-Crystalline $CsPbCl_3$ Perovskite

Microcavities under Multiphoton Excitation. *J. Phys. D Appl. Phys.* **2017**, *50* (22), 225101.
(65) Park, K.; Lee, J. W.; Kim, J. D.; Han, N. S.; Jang, D. M.; Jeong, S.; Park, J.; Song, J. K. Light−Matter Interactions in Cesium Lead Halide Perovskite Nanowire Lasers. *J. Phys. Chem. Lett.* **2016**, *7* (18), 3703−3710.
(66) Wang, X.; Shoaib, M.; Wang, X.; Zhang, X.; He, M.; Luo, Z.; Zheng, W.; Li, H.; Yang, T.; Zhu, X.; Ma, L.; Pan, A. High-Quality In-Plane Aligned $CsPbX_3$ Perovskite Nanowire Lasers with Composition-Dependent Strong Exciton-Photon Coupling. *ACS Nano* **2018**, *12* (6), 6170−6178.
(67) Yang, L.; Li, Z.; Liu, C.; Yao, X.; Li, H.; Liu, X.; Liu, J.; Zhu, P.; Liu, B.; Cui, T.; Sun, C.; Bao, Y. Temperature-Dependent Lasing of $CsPbI_3$ Triangular Pyramid. *J. Phys. Chem. Lett.* **2019**, *10*, 7056−7061.
(68) Pan, J.; Sarmah, S. P.; Murali, B.; Dursun, I.; Peng, W.; Parida, M. R.; Liu, J.; Sinatra, L.; Alyami, N.; Zhao, C.; Alarousu, E.; Ng, T. K.; Ooi, B. S.; Bakr, O. M.; Mohammed, O. F. Air-Stable Surface-Passivated Perovskite Quantum Dots for Ultra-Robust, Single- and Two-Photon-Induced Amplified Spontaneous Emission. *J. Phys. Chem. Lett.* **2015**, *6* (24), 5027−5033.
(69) Xing, G.; Mathews, N.; Lim, S. S.; Yantara, N.; Liu, X.; Sabba, D.; Grätzel, M.; Mhaisalkar, S.; Sum, T. C. Low-Temperature Solution-Processed Wavelength-Tunable Perovskites for Lasing. *Nat. Mater.* **2014**, *13* (5), 476−480.
(70) Buin, A.; Comin, R.; Xu, J.; Ip, A. H.; Sargent, E. H. Halide-Dependent Electronic Structure of Organolead Perovskite Materials. *Chem. Mater.* **2015**, *27* (12), 4405−4412.

https://doi.org/10.1021/acsanm.5c04170
ACS Appl. Nano Mater. 2025, 8, 23933−23944